

Stability and Signatures of Biexcitons in Carbon Nanotubes

Thomas G. Pedersen* and Kjeld Pedersen

Aalborg University, Department of Physics and Nanotechnology,
Pontoppidanstræde 103, DK-9220 Aalborg Øst, Denmark

Horia D. Cornean

Aalborg University, Department of Mathematical Sciences, Fredrik Bajers Vej 7G,
DK-9220 Aalborg Øst, Denmark

Pierre Duclos

CPT-CNRS, Luminy Case 907, F-13288 Marseille Cedex 9, France

Received November 16, 2004; Revised Manuscript Received January 7, 2005

ABSTRACT

The linear optical properties of semiconducting carbon nanotubes are dominated by quasi-one-dimensional excitons formed by single electron–hole pairs. Hence, the nonlinear response at high pump levels most likely leads to the formation of exciton complexes involving several electron–hole pairs. Such complexes would therefore play an important role in, e.g., lasing applications. We demonstrate here that the biexciton complex is surprisingly stable for nanotubes in a wide diameter range. Theoretical predictions for the signature of such states in pump–probe spectroscopy are presented.

Introduction. Strongly bound, quasi-one-dimensional excitons are believed to play an important role in the optical properties of semiconducting single-walled carbon nanotubes (NTs).^{1–5} Experiments applying the micelle-coating technique to isolate individual NTs have revealed highly structured absorption and luminescence spectra^{6–7} and made it possible to assign spectral features to particular NTs according to diameter and chirality.⁷ Resonances in these spectra are interpreted as one-dimensional excitons, and very large exciton binding energies have been predicted in both *ab initio*^{1–3} and effective-mass^{4,5} calculations. Excellent agreement with experimental results for some smaller NTs have been found in *ab initio* calculations,¹ and a pronounced correlation with experimental resonances for a wide range of NTs have been obtained in the effective-mass approach.⁵ A remarkable feature of the experimental results is the small inhomogeneous broadening, which is only around 25–50 meV.⁶ With sufficiently small broadening, it becomes possible to experimentally observe multiparticle excitations. Such states are produced in multiphoton processes and they are likely to be of importance if sufficiently high pumping levels are achieved in, e.g., laser applications. In the present letter, we demonstrate theoretically that biexcitons, i.e., bound complexes formed by two excitons, are surprisingly stable.

Thus, a biexciton binding energy exceeding the inhomogeneous exciton line width (and therefore also the thermal energy at room temperature) is predicted for a wide range of NTs. The implication is that biexcitons should be observable in pump–probe experiments, and we provide calculated signatures of biexciton effects in transient induced absorption spectra.

Biexcitons have previously been observed in other quasi-one-dimensional materials such as conjugated polymers⁸ and quantum wires.⁹ The present results based on an effective-mass model indicate that similar observations can be expected for NTs. Obviously, an effective-mass model is less reliable than *ab initio* approaches. However, at present *ab initio* approaches cannot handle the computational complexity of such four-particle states. Furthermore, the effective-mass model has been found to be in excellent agreement with *ab initio* results for the exciton binding energy and its scaling with NT diameter² as well as the exciton wave function.³ Hence, the effective-mass model presumably provides an efficient and reliable approximation to the full problem. Regarding the possibility of experimentally observing biexcitons, several ultrafast optical techniques are applicable. These all rely on photoinduced modifications of the optical susceptibility probed in frequency or time domain. To address the experimental signatures of biexcitons in NTs, we calculate a pump–probe spectrum corresponding to the

* Corresponding author. E-mail: tgp@physics.aau.dk.

outcome of frequency-resolved pump–probe spectroscopy. Ultrafast measurements of photoinduced bleaching in isolated NTs using one-color or fixed two-color schemes have already been reported.^{10,11} However, ultrafast pump–probe measurements capable of detecting biexcitons should presumably (1) apply a pump photon energy matching the fundamental exciton resonance E_{11} combined with a spectrally resolved probe, and (2) apply samples containing a high concentration of isolated single-walled NTs. Such measurements are still not available. Recently, Korovyanko et al. reported such spectrally resolved results for NT films.¹² The broad features observed in both absorption and transient spectra show, however, that broadening in these samples is too large to resolve biexcitonic effects. Also, Rubtsov et al.¹³ and Ostojic et al.¹⁴ have recently presented frequency-resolved pump–probe measurements. The pump photon energies applied, however, are outside the infrared range in which the fundamental exciton can be excited and, possibly, reexcited in order to create a biexciton. Thus, verification of the predicted biexciton effects must await future refined measurements.

Theory. As in our previous work,^{4,5} electrons and holes in NTs are approximated by carriers confined to the surface of an infinitely long cylinder of radius r as shown in Figure 1. For sufficiently narrow cylinders ($r \ll a_B^*$, the effective Bohr radius), the carriers are completely delocalized around the circumference of the cylinder and an effective Coulomb interaction can be constructed as follows:

$$V(\rho_{||}) = -\frac{1}{2\pi r} \int_0^{2\pi r} \frac{2}{[4r^2 \sin^2(\rho_{\perp}/2r) + \rho_{||}^2]^{1/2}} d\rho_{\perp} = -\frac{4}{\pi|\rho_{||}|} K\left(-\frac{4r^2}{\rho_{||}^2}\right) \quad (1)$$

where $\rho_{||}$ and ρ_{\perp} denote the separation between the carriers along the NT axis and around the circumference, respectively, and K is the elliptic integral. To describe a biexciton state, we consider two electron–hole pairs on the cylinder, cf. Figure 1. When the center-of-mass motion is eliminated and equal electron and hole masses are assumed, the biexciton Hamiltonian is given by

$$H(x,y,z) = -\frac{\partial^2}{\partial x^2} - \frac{\partial^2}{\partial y^2} - \frac{\partial^2}{\partial z^2} + \frac{\partial^2}{\partial x \partial z} - \frac{\partial^2}{\partial y \partial z} + V(x) + V(y) + V(x+z) + V(y-z) - V(z) - V(x+z-y) \quad (2)$$

Here, x and y are the internal electron–hole separations for the individual excitons and z denotes the separation between the holes of the two pairs. Among the four particles, two repulsive and four attractive interactions exist giving a total of six Coulomb terms in eq 2. The biexciton Hamiltonian above has been written in natural exciton units, i.e., length and energy are measured in units of the effective Bohr radius a_B^* and Rydberg R_y^* , respectively.⁴ To obtain the eigenstates of this Hamiltonian, we note that the following symmetries exist: $H(x,y,z) = H(-y, -x, z) = H(y - z, x + z, z)$. Hence, a natural choice for the expansion of the biexciton wave

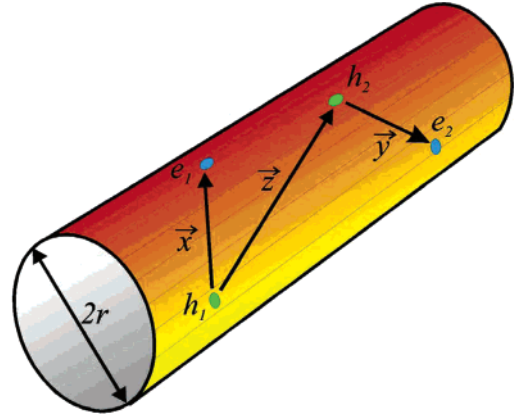


Figure 1. Geometry of the biexciton state on the surface of a cylinder.

function $\Psi(x,y,z) = \sum_{klm} c_{klm} \psi_{klm}(x,y,z)$ is the form

$$\psi_{klm}(x,y,z) = \{\varphi_k(x)\varphi_l(y) + \varphi_k(x+z)\varphi_l(y-z)\}\varphi_m(z) \quad (3)$$

where φ_k is an even function for which we have chosen a Gaussian $\varphi_k(x) = e^{-\alpha_k x^2}$. We can then reduce the problem to the matrix eigenvalue equation

$$(\vec{K} + \vec{U}) \cdot \vec{c} = E \vec{S} \cdot \vec{c} \quad (4)$$

where \vec{S} , \vec{K} and \vec{U} contain overlap, kinetic energy, and potential energy matrix elements, respectively. Using eq 3, relatively simple expressions are obtained for the elements of \vec{S} and \vec{K} , whereas \vec{U} involves the Meijer G-function G_{23}^{22} .

All distances and energies above are given in units of the effective Bohr radius $a_B^* = 0.529 \text{ \AA} \cdot \epsilon/\mu$ and effective Rydberg $R_y^* = 13.6 \text{ eV} \cdot \mu/\epsilon^2$, where ϵ is the dielectric function and $\mu \approx m^*/2$ is the reduced effective mass with m^* the effective carrier (electron or hole) mass. Thus, to convert the theoretical results into physical units, μ must be evaluated from the curvature of the band structure at the band gap for each particular NT, and a_B^* , in fact, becomes roughly proportional to the physical diameter of the NT.⁴ As a consequence, the quantity r , i.e., the NT radius in units of a_B^* , is approximately constant, and from an evaluation of all semiconducting nanotubes with physical diameters in the range 6–16 Å we find $r \in [0.086, 0.135]$ assuming screening by a dielectric constant of $\epsilon = 3.5$. Thus, a typical value is $r = 0.1$, and to find optimal exponents $\{\alpha_k\}$ for the Gaussian expansion we first considered this case. Using a total of six Gaussians, the optimal exponents are $\alpha_k = \{0.27, 1.7, 6.0, 23, 250, 1000\}$. Other values of r are subsequently handled by scaling these values by a factor $(0.1/r)^{1/2}$.

Results. The 6³ dimensional eigenvalue problem eq 4 is solved using the Gaussian basis for r in the range 0.05–0.25. In Figure 2, we plot the biexciton binding energy E_{XX} defined as $E_{XX} = 2E_X - E$, where E_X is the binding energy of a single exciton (obtained from the two-particle analogy of eq 2) and E is the eigenvalue of eq 2. Hence, a positive E_{XX} indicates that the biexciton is stable with respect to

dissociation into two separate excitons. The solid line in Figure 2 is a fit to the form $E_{XX} \approx c/r$ with $c = 0.095$. Hence, it is seen from the quality of the fit that the biexciton binding energy is quite accurately approximated by an inverse dependence on r , except perhaps for the smallest values of r . This, in turn, means that when converted into eV, the dependence of E_{XX} on μ is practically canceled, i.e.,

$$E_{XX}[\text{in eV}] \approx \frac{0.095}{r[\text{in } \text{\AA}]/a_B^*} \cdot R_y^* = \frac{0.095 \times 13.6 \text{ eV} \times 0.529 \text{ \AA}}{r[\text{in } \text{\AA}]\epsilon} \approx \frac{0.195 \text{ eV}\text{\AA}}{r[\text{in } \text{\AA}]} \quad (5)$$

Hence, the actual biexciton binding energy is inversely proportional to the physical NT radius. Note that independence of μ is a highly special case, which is obtained only for an r^{-1} dependence of the energy. The results after conversion into eV and \AA are depicted in the inset of Figure 2 for the diameter range 6–16 \AA . Obviously, the predicted biexciton binding energies in NTs are extremely large compared to typical values for inorganic nanostructures such as $\text{In}_x\text{Ga}_{1-x}\text{As}/\text{GaAs}$ quantum wires in which E_{XX} is at least 10 times smaller.⁹

The striking prediction of the calculations is that the biexciton binding energy is larger than or roughly equal to both the inhomogeneous broadening⁶ and the room temperature thermal energy for most NTs in the range of physical diameters found in typical samples. Under this condition, pump–probe spectra are expected to reveal the presence of biexcitons as a photoinduced absorption peak accompanying the exciton resonance and red-shifted from it by the biexciton binding energy. Diagrammatic summation shows that the correction to the long-axis susceptibility induced by an intense pump beam at frequency ω_2 and probed at frequency ω_1 is given by¹⁵

$$\chi^{(3)} = \chi_0 \left[\frac{1}{\omega_1 - \omega_0 + i\Gamma} - \frac{1}{\omega_1 - \omega_0 + E_{XX}/\hbar + i\Gamma} \right] \times \left[\frac{\omega_1 - \omega_2 + 2i\Gamma}{(\omega_1 - \omega_0 + i\Gamma)(\omega_0 - \omega_2 + i\Gamma)(\omega_1 - \omega_2 + i\Gamma)} - \frac{2}{(\omega_2 - \omega_0)^2 + \Gamma^2} \right] \quad (6)$$

where $\hbar\omega_0$ is the exciton energy, χ_0 is a frequency-independent constant for each NT type, and identical longitudinal and transverse broadening (Γ) has been assumed. The first and second terms of the first square bracket are responsible for bleaching due to depopulation of the ground state and photoinduced absorption via exciton to biexciton transitions, respectively. In Figure 3, both of these effects are clearly visible as signatures in the photoinduced absorption spectrum $-\text{Im}\{\chi^{(3)}\}$. Here, a (6,4)-NT (radius 3.46 \AA) has been considered for which the biexciton binding energy predicted by eq 5 is 56 meV and the experimentally measured energy of the fundamental exciton is 1.42 eV.⁷ The case of resonant pumping is shown, i.e., $\omega_2 = \omega_0$ and three different

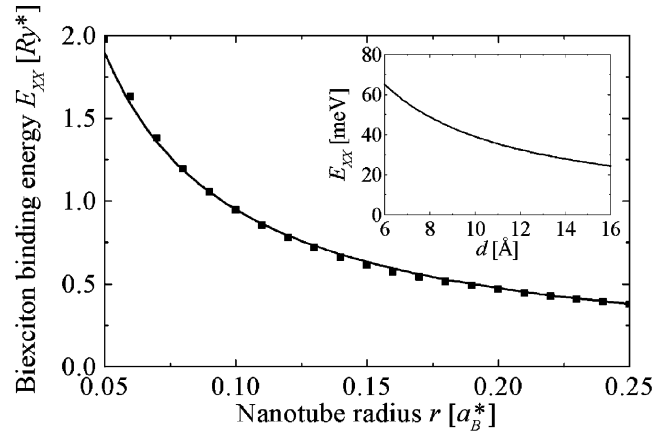


Figure 2. Biexciton binding energy vs NT radius, both in natural exciton units. The solid curve is a fit to an r^{-1} dependence. Inset: results converted to physical units, eV and \AA .

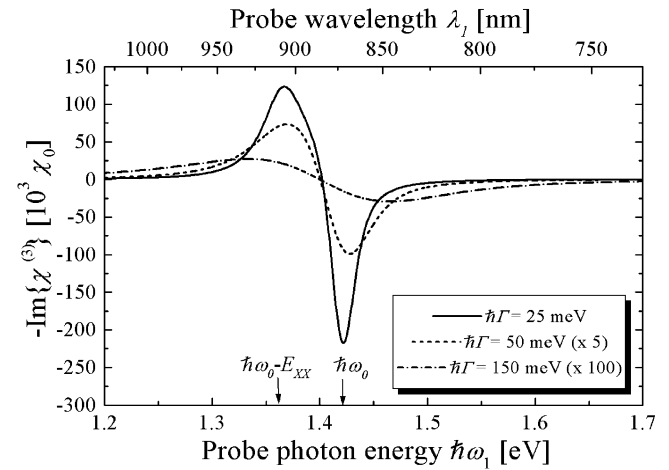


Figure 3. Induced probe absorption spectrum assuming resonant pumping conditions and different values of the inhomogeneous broadening. The curves are for a (6,4)-NT for which $E_{XX} \approx 56$ meV.

values of the broadening are used. The results show that a clearly discernible biexciton peak is found at low broadening. However, at $\hbar\Gamma = 150$ meV the visibility and intensity of the biexciton signature is dramatically decreased, indicating that experimental observation will be difficult if broadening significantly exceeds biexciton binding energy.

Another potential obstacle to experimental verification is that samples always contain a distribution of NTs with different diameters and chiralities. Thus, overlapping contributions from several species are expected in the spectrum. To address this point, we show in Figure 4 the photoinduced absorption spectrum in a two-dimensional pump–probe plot. In this figure, a broadening of 25 meV has been assumed and all NTs with a fundamental exciton resonance between 1.0 and 1.5 eV have been included with equal weight, ignoring the weak dependence of χ_0 on NT species. Each cross in the plot corresponds to a doubly resonant case $\omega_1 = \omega_2 = \omega_0$ for some NT in the ensemble. It is seen that each NT species produces a photobleaching region near resonance as well as a red-shifted photoinduced absorption region due to biexcitons, as expected. However, the proximity

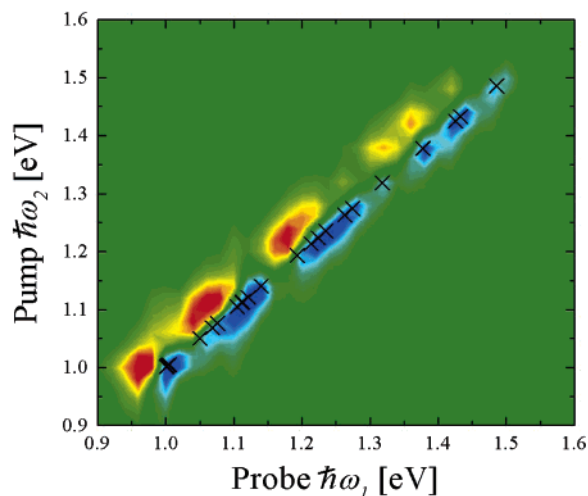


Figure 4. Two-dimensional pump–probe spectrum for an ensemble of NTs with fundamental exciton resonances between 1.0 and 1.5 eV. The color coding illustrates $-\text{Im}\{\chi^{(3)}\}$ in arbitrary units with blue and red as minimum and maximum, respectively.

of the resonances leads to a large overlap between contributions from different NT species. Hence, for a sample with the simulated composition and spectral broadening, biexciton signatures from individual NTs are resolved only for certain species. Even in the case of such a wide distribution of species, though, the presence of biexcitons in the sample should be clearly detectable.

Summary. We have addressed the question of stability of biexcitons in single-walled carbon NTs and the possible experimental observation of such states in pump–probe spectroscopy. A surprisingly large biexciton energy inversely

proportional to NT radius is predicted. The implication of this result is that biexcitons are predicted to be observable as photoinduced absorption features provided broadening is less than biexciton binding energy. Judging from available absorption spectra, this condition should, indeed, be fulfilled for isolated micelle coated NTs.⁶

References

- (1) Spataru, C. D.; Ismail-Beigi, S.; Benedict, L. X.; Louie, S. G. *Phys. Rev. Lett.* **2004**, *92*, 077402.
- (2) Perebeinos, V.; Tersoff, J.; Avouris, Ph. *Phys. Rev. Lett.* **2004**, *92*, 257402.
- (3) Chang, E.; Bussi, G.; Ruini, A.; Molinari, E. *Phys. Rev. Lett.* **2004**, *92*, 196401.
- (4) Pedersen, T. G. *Phys. Rev. B* **2003**, *67*, 073401.
- (5) Pedersen, T. G. *Carbon* **2004**, *42*, 1007–1010.
- (6) O’Connell, M. J.; Bachilo, S. M.; Huffman, C. B.; Moore, V. C.; Strano, M. S.; Haroz, E. H.; Rialon, K. L.; Boul, P. J.; Noon, W. H.; Kittrell, C.; Ma, J.; Hauge, R. H.; Weisman, R. B.; Smalley, R. E. *Science* **2002**, *297*, 593–596.
- (7) Bachilo, S. M.; Strano, M. S.; Kittrell, C.; Hauge, R. H.; Smalley, R. E.; Weisman, R. B. *Science* **2002**, *298*, 2361–2366.
- (8) Klimov, V. I.; McBranch, D. W.; Barashkov, N.; Ferraris, J. *Phys. Rev. B* **1998**, *58*, 7654–7662.
- (9) Baars, T.; Braun, W.; Bayer, M.; Forchel, A. *Phys. Rev. B* **1998**, *58*, R1750–R1753.
- (10) Arnold, M. S.; Sharping, J. E.; Stupp, S. I.; Kumar, P.; Hersam, M. C. *Nano Lett.* **2003**, *3*, 1549–1554.
- (11) Huang, L.; Pedrosa, H. N.; Krauss, T. D. *Phys. Rev. Lett.* **2004**, *92*, 17403.
- (12) Korovyanko, O. J.; Sheng, C. X.; Vardany, Z. V.; Dalton, A. B.; Baughman, R. H. *Phys. Rev. Lett.* **2004**, *92*, 017403.
- (13) Rubtsov, I. V.; Russo, R. M.; Albers, T.; Deria, P.; Luzzi, D. E.; Therien, M. J. *Appl. Phys. A* **2004**, *79*, 1747.
- (14) Ostojic, G. N.; Zaric, S.; Kono, Z.; Moore, V. C.; Hauge, R. H.; Smalley, R. E. *cond-mat/0408667*.
- (15) Madarasz, F. L.; Szmulowicz, F.; Hopkins, K.; Dorsey, D. L. *Phys. Rev. B* **1994**, *49*, 13528–13541.

NL048108Q